Reduction and compensation of the transient beam loading effect in a double rf system of synchrotron light sources

Naoto Yamamoto,* Takeshi Takahashi, and Shogo Sakanaka

Accelerator Laboratory, High Energy Accelerator Research Organization (KEK), 1-1 Oho, Tsukuba, Ibaraki 305-0801, Japan

(Received 21 August 2017; published 3 January 2018)

Double rf systems are used to lengthen the beam bunches in synchrotron light sources. In such a system, the performance of the bunch lengthening is limited by the transient beam-loading effect, which is induced by gaps in the fill pattern. To improve its performance, we investigate an application of a normal-conducting harmonic cavity, which is based on the TM020 resonant mode. By using the TM020 mode with low R/Q and high Q, fluctuation of the rf voltage due to the transient beam loading can be reduced significantly. The remaining small fluctuation of the rf voltage can be compensated by using an active feedforward technique. Using these measures, we expect to realize a bunch-lengthening performance that is comparable to that obtained with superconducting cavities under realistic operational parameters of a proposed 3-GeV next-generation light source. We estimate the bunch-lengthening performances using macroparticle tracking simulations together with semianalytical calculations.

DOI: 10.1103/PhysRevAccelBeams.21.012001

I. INTRODUCTION

Quasidiffraction-limited synchrotron light sources, which aim at achieving horizontal beam emittances of ∼100 pm rad or lower, have been constructed or are being actively designed [1]. In such ultralow-emittance storage rings, emittance growth due to intrabeam scattering, as well as a short Touschek lifetime, are serious concerns [2], especially in the low-to-medium energy range. To mitigate such adverse effects, a double radio-frequency (rf) system [3] is used to lengthen the beam bunches, using which the particle densities at the core of the bunches can be reduced. In a typical double rf system, the third or fourth harmonic rf voltage is applied to the beam in order to cancel the slope of the main rf voltage.

Double rf systems have been installed in several third-generation light sources, and they have been successfully operated to lengthen beam bunches [4–11], resulting in longer Touschek lifetimes. However, among these works, the bunch-lengthening performances were limited when normal-conducting (NC) cavities were used at a high harmonic frequency of 1.5 GHz [4,6]. This limitation was caused by the transient beam-loading effect in the harmonic cavities [12]. When the gaps, i.e., unoccupied rf buckets, were introduced in the fill pattern of the stored beam, the bunch gaps induced considerable variations in both amplitude and phase in the harmonic rf voltage. The bunches were then largely influenced by such transient voltages owing to the absence of the longitudinal focusing force. This effect is important when the harmonic frequencies are high, that is, typically higher than 1 GHz. It was reported [12] that the reduction of a total R/Q of harmonic cavities is essential to alleviate such transient effects. For this reason, superconducting (SC) cavities have been considered to be the most suitable choice for the harmonic cavities, especially at high harmonic frequencies. SC harmonic cavities have been installed in several storage rings, and they have been successfully operated [7–9].

Recently, a novel damped accelerating cavity with a resonant frequency of 508.6 MHz was developed by Ego *et al.* [13,14]. In this cavity, the TM020 resonant mode is used for beam acceleration. Because the TM020 mode has a node of magnetic fields at a certain location in the radial direction, they located annular slots for extracting unwanted parasitic modes at these locations of the end walls of the cavity. With the exception of the TM020 mode, the parasitic modes can strongly couple to these slots, and they can be damped by microwave absorbers that fit in the slots. In this scheme, effective parasitic-mode damping is possible while maintaining the compact longitudinal size of the cavity. Another advantage of this cavity is its low R/Q and high unloaded Q. We considered that by using a similar TM020-mode cavity with the harmonic rf system, the bunch-lengthening performance will be significantly improved.

With this concept, we studied the possibilities of a normal-conducting double rf system. We aimed to lengthen the beam bunches, thus improving the beam performances,

*naoto.yamamoto@kek.jp

in a 3-GeV next-generation light source, i.e., the KEK Light Source (KEK-LS) [15,16], which is currently under consideration. In Sec. II, we introduce a TM020-mode cavity for our harmonic cavity. We then present the operational principles of our proposed double rf system, and show the parameters that are assumed. In Sec. III, we present our estimations of the bunch lengths and transient rf voltages. First, we describe our simulation code and show the calculation results. Then, we present other calculations that are based on a semianalytical method and show that these results agree well with the tracking simulations. In Sec. IV, we show that the bunch lengthening can be further improved by using active compensation techniques. In Sec. V, we compare the bunch lengths and transient voltages that are expected with our method to those with SC cavities. Finally, in Sec. VI, we present our conclusions.

II. DOUBLE RF SYSTEM

A. TM020-mode cavity

Figure 1 shows a 1.5-GHz harmonic cavity that we assumed for our investigation. Based on the pioneering work by Ego *et al.*, we use the TM020 mode to produce the harmonic rf voltage. The other parasitic modes, including the fundamental TM010 mode, are damped by equipping either annular slots [13] or HOM couplers [17]. However, for the current study, we did not include these mechanisms, and we assumed the cavity parameters without them. Table I shows the principal parameters of the TM020 cavity, which were calculated using the SUPERFISH code [18]. The cavity shown in Fig. 1 has an R/Q of 77.2 Ω, and an unloaded Q of 37,500. Compared to existing 1.5-GHz NC cavities [4–6] that are based on the conventional TM010 mode, R/Q is about one half and the unloaded Q is higher by a factor ranging from 1.5 to 3.

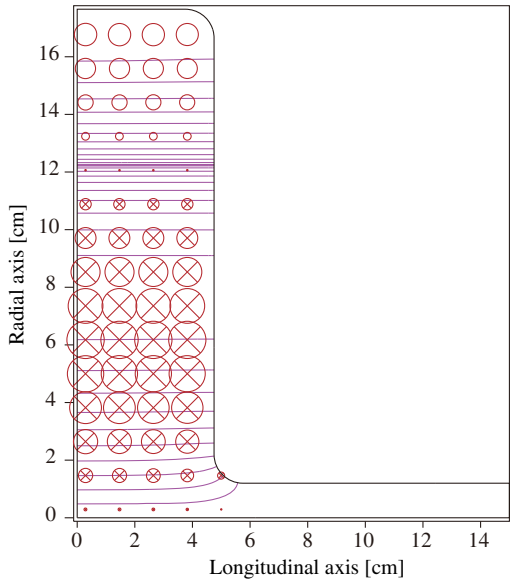

FIG. 1. Inner shape (in z-r plane) of the 1.5-GHz TM020-mode cavity. Only a half of the cavity is shown. Lines and circles indicate the electric and magnetic fields, respectively.

TABLE I. Principal parameters of the TM020 cavity which were assumed for our investigation.

Parameter	Symbol	Value
Resonant frequency	f_{res}	1.500 GHz
Shunt impedance[a] divided by Q	R/Q	77.2 Ω
Unloaded Q	Q_0	37 500
Shunt impedance[a]	R	2.90 MΩ
Inner radius	-	176.5 mm
Gap length	-	95 mm
Maximum power dissipated on the cavity wall	$P_{c,\mathrm{max}}$	10 kW
Cavity voltage at $P_{\mathrm{c,max}}$	$V_{\mathrm{c,cell}}$	170 kV
Max. electric field on the inner surface	E_{max}	3.2 MV/m
Max. power density on the inner surface	ρ_{max}	10.0 W/cm^2

[a]The shunt impedance is defined by $R = V_{\mathrm{c}}^2/P_{\mathrm{c}}$.

B. Operational principles and notations

We assume the use of a double rf system to lengthen the bunches in the planned KEK-LS. We utilize a main radio frequency of 500 MHz and the third harmonic frequency of 1.5 GHz. Detailed parameters are shown in Sec. II C.

With the double rf system, which comprises the main and nth harmonic rf systems, the total rf voltage seen by a particle is given by

$$V(\phi) = V_{\mathrm{c},1}\cos(\phi + \phi_1) + V_{\mathrm{c},n}\cos(n\phi + n\phi_n), \quad (1)$$

where ϕ is the phase angle of the particle with respect to the main rf wave ($\phi > 0$ implies that the particle passes the cavities after the synchronous particle), ϕ_1 and $n\phi_n$ are the synchronous phases with respect to the main and harmonic rf waves, respectively, and $V_{\mathrm{c},1}$ and $V_{\mathrm{c},n}$ are the main and harmonic rf voltages, respectively. In this paper, the subscript n denotes the parameters related to the nth harmonic rf, where $n = 1$ stands for the main rf. To ensure that all numerical expressions are compatible with those of P.B. Wilson's textbook [19], we adopted the cosine function in Eq. (1). Synchrotron oscillation is stable when ϕ_1 is in the first quadrant ($0 < \phi_1 < \pi/2$). Then, we can show that the $n\phi_n$ should be in the third quadrant ($-\pi < n\phi_n < -\pi/2$) if the harmonic cavity is driven by beams (i.e., deceleration) and if the slope of the harmonic rf cancels that of the main rf, at the synchronous phases.

To lengthen the bunches, we require the flat potential condition, $V'(0) = 0$ and $V''(0) = 0$ [3,11,12]. Then, the parameters ϕ_1, $n\phi_n$, and the voltage ratio k, are determined by

$$\cos\phi_1 = \frac{n^2}{n^2 - 1}\frac{U_0}{e_0 V_{\mathrm{c},1}}, \quad (2)$$

$$\tan n\phi_n = n \tan \phi_1, \tag{3}$$

and

$$k \equiv \frac{V_{c,n}}{V_{c,1}} = -\frac{\sin \phi_1}{n \sin(n\phi_n)}, \tag{4}$$

where U_0 is the synchrotron radiation loss per turn in electron volts, and e_0 is the elementary charge (we assume $e_0 > 0$).

We assume to connect each harmonic cavity to an external rf generator with a coupling coefficient of β_n. The tuning angle of the harmonic cavity is defined by

$$\begin{aligned}\tan \psi_n &\equiv -Q_{L,n}\left(\frac{n\omega_{rf}}{\omega_{res,n}} - \frac{\omega_{res,n}}{n\omega_{rf}}\right) \\ &\approx 2Q_{L,n}\frac{\omega_{res,n} - n\omega_{rf}}{\omega_{res,n}},\end{aligned} \tag{5}$$

where ω_{rf} is the main angular radio frequency, $\omega_{res,n}$ is the angular resonant frequency of the harmonic cavity, and $Q_{L,n} = Q_{0,n}/(1+\beta_n)$ is the loaded Q of the harmonic cavity with $Q_{0,n}$, which is the unloaded Q. We take ψ_n in the range of $-\pi/2 < \psi_n < \pi/2$.

We assume that at the maximum beam current of $I_{0,max}$, the harmonic cavities are driven only by beams, i.e., the passive operation. A typical phasor diagram in this situation is shown in Fig. 2(a). To produce the harmonic rf voltage

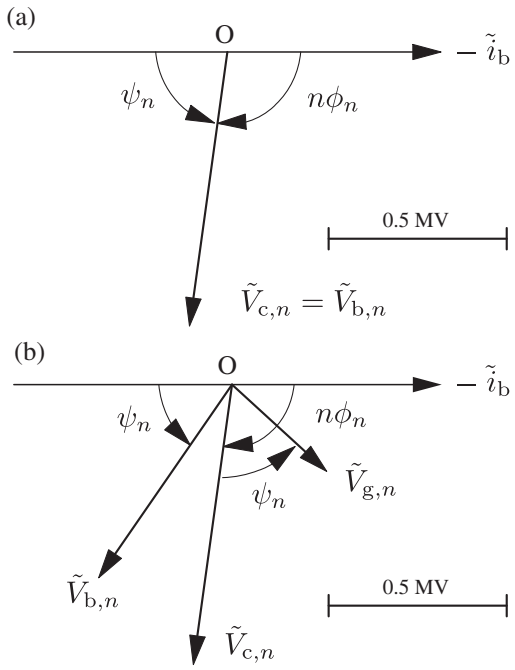

FIG. 2. Typical phasor diagrams showing rf voltages in the harmonic cavities. (a) At a maximum beam current of 500 mA, (b) at a beam current of 100 mA. Assumed parameters are given in Sec. II C. Note that the direction of the beam induced voltage at resonance, $\tilde{V}_{br}$, is opposite to that of the $-\tilde{i}_b$.

required from Eqs. (3) and (4), the following relations are needed:

$$\psi_n = n\phi_n + \pi, \tag{6}$$

and

$$-\frac{I_{0,max}R_n \cos(n\phi_n)}{1+\beta_n} = V_{c,n}, \tag{7}$$

where R_n is the total shunt impedance of the harmonic cavities. In Eq. (7), we assumed that the bunch lengths are much shorter than the rf wavelength, and we set a bunch form factor F to be 1. For a given shunt impedance, we choose the coupling coefficient such that Eq. (7) holds, and we detune the harmonic cavities such that Eq. (6) is satisfied. In the case where the Eq. (7) does not hold for any value of β_n, we modify the shunt impedance R_n by changing the number of cavities, or by other means.

At a lower beam current, the harmonic cavities are partly driven by the external generators in order to keep the cavity voltage unchanged. The cavity voltage $\tilde{V}_{c,n}$ is then the sum of the beam-induced voltage $\tilde{V}_{b,n}$ and the generator-induced voltage $\tilde{V}_{g,n}$. A typical phasor diagram is shown in Fig. 2(b). In this situation, we adjust the tuning angle so that the cavity impedance seen by the generator becomes real. This is satisfied when the tuning angle is adjusted according to the relation [19],

$$\tan \psi_n = -\frac{I_0 R_n}{V_{c,n}(1+\beta_n)} \sin(n\phi_n), \tag{8}$$

where I_0 is the beam current. The power required for the generator is then given by

$$P_{g,n} = \frac{(1+\beta_n)^2}{4\beta_n}\frac{(V_{c,n})^2}{R_n}\left[1 + \frac{I_0 R_n}{V_{c,n}(1+\beta_n)}\cos(n\phi_n)\right]^2. \tag{9}$$

Note that at the maximum current, Eqs. (8)–(9) are consistent with Eqs. (6)–(7).

When the gaps are introduced in the fill pattern of the stored beam, the cavity voltage fluctuates owing to the transient effect. In this situation, we set an average cavity voltage $(\tilde{V}_{c,n})_{av}$ over a bunch train to be equal to the voltage required for the flat potential condition. To do this, we adjust the generator voltage $\tilde{V}_{g,n}$ slightly. The generator voltage is primarily kept constant at a given beam current, except for the use of active compensation techniques (see Sec. IV).

C. Parameters of the KEK-LS

Table II shows the principal parameters of the KEK-LS that were assumed for our investigation. In a standard operation, all rf buckets will be equally filled with

TABLE II. Principal parameters of the KEK-LS, which were assumed in this study.

Parameter	Symbol	Value
Nominal beam energy	E_0	3.0 GeV
Stored beam current	I_0	500 mA
Radio frequency (fundamental)	f_{rf}	500.07 MHz
Harmonic number	h	952
Revolution frequency	f_0	525 kHz
Unperturbed synchrotron frequency[a]	f_{s0}	2.65 kHz
Synchrotron radiation loss per turn[b]	U_0	851 keV
Main rf voltage	$V_{c,1}$	2.5 MV
Natural relative energy spread[b] (rms)	σ_ϵ	7.3×10^{-4}
Momentum compaction factor	α_c	2.2×10^{-4}
Longitudinal radiation damping time[b]	τ_ϵ	7.0 ms
Natural bunch length[ab] (rms)	σ_τ	9.5 ps

[a]Without harmonic cavities.
[b]Including insertion devices.

electrons, except for the bunch gaps. To avoid ion trapping, we introduce several bunch gaps symmetrically in the ring. The number and duration of the gaps are tentatively 2 and 60 ns, respectively. Then, the ring is filled with two bunch trains, each comprising 446 bunches, and the bunch trains are spaced by 30 empty buckets. We refer to this as the standard fill pattern of the KEK-LS. In order to keep the charge in every bunch, we assume the "top-up" operation. Note that the Photon Factory storage ring at KEK was recently (April, 2017) operated with four 64-ns bunch gaps to avoid some beam instabilities, and the assumed gap duration of 60 ns is similar to this operation.

For the cavities of the main rf system, we primarily assumed the use of existing Photon Factory (PF-) type cavities [20]. This cavity has a resonant frequency of 500 MHz, an unloaded Q of 40,000, and an R/Q of 175 Ω. To produce a typical main rf voltage of 2.5 MV, five cavities are needed. The total R/Q amounts to 875 Ω. The transient voltage variation in these cavities was estimated to be about 1.6% peak-to-peak, which is about a quarter of that in the harmonic cavities. Then, the transient effects are primarily dominated by the harmonic cavities. In Sec. V, we discuss the other cases involving the use of the SC cavities.

TABLE III. Principal parameters of the double rf system for the KEK-LS at the beam current of 500 mA. For the main and harmonic cavities, the PF-type cavity and the TM020 cavity were assumed, respectively.

Parameter	Symbol	Main rf ($n = 1$)	Harmonic rf ($n = 3$)
Rf voltage	$V_{c,n}$	2.5 MV	777 kV
Synchronous phase	$n\phi_n$	1.178 rad	−1.708 rad
Tuning angle	ψ_n	−0.962 rad	1.433 rad
Total R/Q	R_n/Q	875 Ω	386 Ω
Total shunt impedance	R_n	35 MΩ	14.48 MΩ
Cavity coupling coefficient	β_n	3.5	0.27
Cavity detuning amount	$\Delta f_{\mathrm{res},n}$	−40.3 kHz	185 kHz
Total generator power	$P_{g,n}$	657 kW	0.0 kW
Total reflected power	$P_{r,n}$	0.4 kW	11.4 kW

For the third harmonic rf system, we assumed the TM020-mode cavities shown in Fig. 1. We use five cavities to produce a typical harmonic voltage of 777 kV. With respect to Table I, the total R/Q amounts to 386 Ω. Under a typical rf voltage of 155 kV per cavity, both the electric field and the dissipated power density on the inner wall are conventional as shown in Table I.

Table III shows the operational parameters of the double rf system, which gives the flat potential condition at the maximum beam current of 500 mA when the ring is filled uniformly. With the bunch gaps, the generator voltage $\tilde{V}_{g,n}$ is slightly modified, as was mentioned in Sec. II B.

III. EVALUATION OF BUNCH LENGTHENING

A. Method of tracking simulation

To evaluate the bunch lengths under the transient beam loading, we developed a tracking simulation code. In our simulation, each stored bunch is represented by a collection of macroparticles. We usually employed 1,000 macroparticles per bunch, and about 10^6 macroparticles per ring. The longitudinal motions of these macroparticles were simulated while considering their interaction with the main and harmonic rf cavities. The other interactions, such as those with the ring coupling impedances or with ions, were currently not included. With this method, the distribution of electrons in every bunch can be calculated from the first principle, and the results are suitable for checking the other approximate evaluations. When compared to similar codes [11,12,21,22], our simulation can include the active compensation techniques that are described in Sec. IV.

In the simulation, the synchrotron motion of a macroparticle is described by the phase angle ϕ and the relative energy deviation from the nominal energy, ε. We use an index i to indicate a macroparticle in a bunch, and we use an index j for the number of turns. While the ith macroparticle circulates the ring besides the cavities, its variables change according to the relations:

$$\phi^{(i,j)} = \phi^{(i,j-1)} + 2\pi\alpha_c h\varepsilon^{(i,j-1)}, \tag{10}$$

and

$$\varepsilon^{(i,j)} = \varepsilon^{(i,j-1)}\left(1 - \frac{2}{\tau_\varepsilon f_0}\right) - \frac{U_0}{E_0} + Q_\varepsilon, \tag{11}$$

where α_c is the momentum compaction factor, h is the harmonic number, τ_ε is the longitudinal radiation damping time, f_0 is the revolution frequency, and E_0 is the nominal beam energy in electron volts. Q_ε is a random number that represents the quantum fluctuation, and it is determined according to the normal distribution having the

characteristics of $\langle Q_\varepsilon \rangle = 0$ and $\langle {Q_\varepsilon}^2 \rangle = 4{\sigma_\varepsilon}^2/(\tau_\varepsilon f_0)$, where σ_ε is the relative rms energy spread of the beam. Note that the parameters σ_ε and τ_ε, are determined by the accelerator design, and are given as input parameters.

When a macroparticle passes the nth harmonic cavities, it induces an additional rf voltage in the cavities. We employ a variable $\tilde{V}_{b,n}^{(i,j)}$ to indicate the beam-induced voltage just before the passage of the ith macroparticle at the jth turn. We assume that the indices is are aligned according to the arrival time of the macroparticles. Then, the change in the beam-induced voltage between the arrival of (i-1)th and ith macroparticles is given by

$$\tilde{V}_{\mathrm{b},n}^{(i,j)} = (\tilde{V}_{\mathrm{b},n}^{(i-1,j)} - 2k_n q_\mathrm{M}) \exp\{\alpha_n \Delta t^{(i)}\}, \quad (12)$$

with

$$\alpha_n = -\frac{1}{\tau_{\mathrm{f},n}}(1 - i\tan\psi_n), \quad (13)$$

where $k_n = (\omega_{\mathrm{res},n}/4)(R_n/Q)$ is the total loss parameter of the nth harmonic cavities, q_M is the charge of the macroparticle, $\Delta t^{(i)}$ is the time interval between the (i-1)th and ith macroparticles, and $\tau_{\mathrm{f},n} = 2Q_{\mathrm{L},n}/\omega_{\mathrm{res},n}$ is the cavity filling time. The i on the right-hand side of Eq. (13) denotes the imaginary unit. We also repeat similar calculations for different bunches.

The cavity voltage is given by $\tilde{V}_{\mathrm{c},n}^{(i,j)} = \tilde{V}_{\mathrm{g},n} + \tilde{V}_{\mathrm{b},n}^{(i,j)}$, where $\tilde{V}_{\mathrm{g},n}$ is the generator-induced voltage. The $\tilde{V}_{\mathrm{g},n}$ is determined so that an average cavity voltage over a bunch train becomes equal to the voltage required from the flat potential condition. In cases where the active compensation is applied, we change the $\tilde{V}_{\mathrm{g},n}$ so that it depends on the indices (i, j). Once the cavity voltage has been calculated, the energy gain of the macroparticle owing to the passage of the main and harmonic cavities is given by

$$\varepsilon^{(i,j)} = \varepsilon^{(i,j-1)} + \frac{e_0}{E_0}\{\mathrm{Re}[\tilde{V}_{\mathrm{c},1}^{(i,j)} \exp(i\phi^{(i,j)})] + \mathrm{Re}[\tilde{V}_{\mathrm{c},n}^{(i,j)} \exp(in\phi^{(i,j)})] - (k_1 + k_n)q_\mathrm{M}\}. \quad (14)$$

Initially, we set particle distributions and cavity voltages that were close to the operational conditions, and we applied Eqs. (10)–(14) repeatedly until the macroparticles reached steady-state distribution. We then deduced the bunch lengths and transient rf voltages at the steady state.

B. Simulation results

To validate our code, we conducted a tracking simulation using the parameters of a double rf system for the Swiss Light Source [23] where a 1.5-GHz third-harmonic SC cavity was used. Although the total R/Q of the harmonic cavity was as low as 177 Ω, the bunch lengths were significantly affected by the transient beam-loading effect owing to the use of long bunch gap of ∼280 ns. It was reported [23] that the bunch positions shifted by 210 ps in peak-to-peak while the root-mean-square (rms) bunch lengths varied from 24 ps to 66 ps among the bunch train, at a beam current of 320 mA. On the other hand, our simulation predicted the bunch position shifts of 205 ps in peak-to-peak and the rms bunch lengths which ranged from 21 ps to 60 ps, both of which agreed those from the above-mentioned report.

We then conducted the tracking simulations assuming the parameters in Table II. Figure 3 shows the results of the simulations, where the rms length of each bunch is plotted as a function of the bucket index. We first conducted simulations under the conditions, (i) without harmonic cavities or bunch gaps, and (ii) with TM020-mode harmonic cavities and without bunch gaps. The corresponding results are indicated by magenta and green symbols, respectively. Under condition (i), the rms bunch length was 9.48 ps on average, which agreed with the theoretical prediction of 9.50 ps. Under the other condition (ii), the average rms bunch length was approximately 41.8 ps, which agreed with the theoretical prediction of 42.5 ps under an ideal flat-potential condition.

Next, we conducted simulations assuming the standard fill pattern having two bunch gaps of 60 ns each. The fill pattern is shown in the upper inset of Fig. 3. For the third harmonic cavities, we investigated the following cases, (iii) five TM020-mode cavities described in Sec. II A, and (iv) twelve TM010-mode BESSY-II-type harmonic cavities [6]. In case (iii), operational parameters are given in Table III. In case (iv), we assumed the third-harmonic

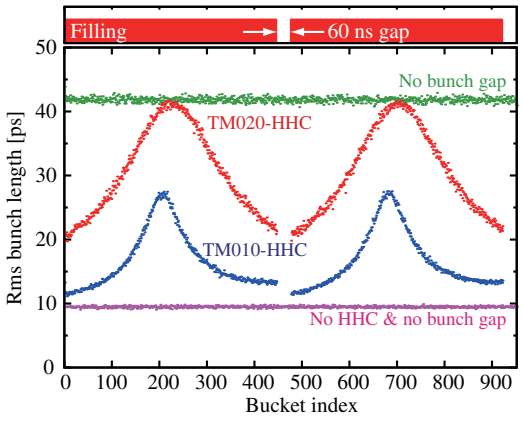

FIG. 3. Results of the tracking simulations showing rms bunch lengths along the bunch trains. Abscissa shows the index of the rf buckets. The upper inset indicates the standard fill pattern of the ring. Symbols in different colors indicate the bunch lengths under the conditions: (magenta) without bunch gap or harmonic cavities, (green) without bunch gap and with the third harmonic cavities, (red) with bunch gaps of 60 ns and using the TM020-mode harmonic cavities, and (blue) with bunch gaps of 60 ns and using BESSY-II-type TM010-mode harmonic cavities.

voltage of 64.8 kV per cavity by referring to a typical operational voltage given in [6]; the total R_n/Q amounted to 1488 Ω. The corresponding results are respectively shown by red and blue symbols in Fig. 3. In these cases, the bunch lengths varied from bunch to bunch owing to the transient effect. When the TM020-mode cavities were assumed, the estimated bunch lengths ranged between 20–42 ps, as indicated by the red symbols. The average rms bunch length was 30.5 ps, which was longer than the natural length by a factor of 3.2. However, if we assumed conventional TM010-mode cavities, the estimated bunch lengths were considerably shorter than the case of the TM020-mode cavities, as indicated by the blue symbols. The average rms bunch length was 16.6 ps, which was longer than the natural length by a factor of 1.7. These simulations demonstrated that the TM020-mode cavities are very effective for lengthening bunches when the bunch gaps are introduced.

C. Method of semianalytical calculation

In order to understand the simulation results better, we tried to explain them analytically using a suitable approximation. This approach also allows us to estimate the bunch lengths quickly while the tracking simulation takes a long time. Note that our approach is similar to the simulation model in [12], except for the calculation of transient rf voltages.

We assume that each bunch is a point charge of q_b, and that the bunches are equally spaced within a bunch train with an interval of t_b $(= 1/f_\mathrm{rf})$. Here, we have ignored the shifts in the bunch centers that are due to transient voltages. We assume that the ring is filled with several bunch trains, each having n_t bunches, and that these bunch trains are spaced by n_g empty buckets.

We pay attention to the fact that the beam-induced voltage under the steady state is periodic with a repetition period, $(n_\mathrm{t}+n_\mathrm{g})t_\mathrm{b}$, of bunch trains. Then, the beam-induced voltage at (just before) the first bunch among the bunch train, $\tilde{V}^{(1)}_{\mathrm{b},n}$, should be equal to that after one period of the bunch train. This relation is expressed by

$$\tilde{V}^{(1)}_{\mathrm{b},n} = \tilde{V}^{(1)}_{\mathrm{b},n} e^{(n_t+n_g)\alpha} + \sum_{l=1}^{n_t} \{-2k_n q_b e^{l\alpha}\} e^{n_g\alpha}, \tag{15}$$

with

$$\alpha = -\frac{t_\mathrm{b}}{\tau_{\mathrm{f},n}}(1 - i\tan\psi_n). \tag{16}$$

Here, the first term in the right-hand side of Eq. (15) represents the changed voltage after the period, and the second term gives the sum of the induced voltages by the bunches among the bunch train. Then, the steady-state beam-induced voltage at (just before) the mth point bunch, where m is counted from the first bunch in the bunch train, is given by

$$\tilde{V}^{(m)}_{\mathrm{b},n} = \tilde{V}^{(1)}_{\mathrm{b},n} e^{(m-1)\alpha} + \sum_{l=1}^{m-1} \{-2k_n q_b e^{l\alpha}\}. \tag{17}$$

From Eqs. (15) and (17), the $\tilde{V}^{(m)}_{\mathrm{b},n}$ is expressed as

$$\tilde{V}^{(m)}_{\mathrm{b},n} = -2k_n q_\mathrm{b} \frac{e^\alpha}{1-e^\alpha} \times \left\{ \frac{1-e^{n_\mathrm{t}\alpha}}{1-e^{(n_\mathrm{g}+n_\mathrm{t})\alpha}} e^{(n_\mathrm{g}+m-1)\alpha} + 1 - e^{(m-1)\alpha} \right\}. \tag{18}$$

The nth harmonic voltage that is applied to the mth point bunch is then given by

$$\tilde{V}^{(m)}_{\mathrm{c},n} = \tilde{V}^{(m)}_{\mathrm{b},n} + \tilde{V}_{\mathrm{g},n} - q_\mathrm{b} k_n. \tag{19}$$

As explained in Sec. III A, the generator-induced voltage $\tilde{V}_{\mathrm{g},n}$ is determined so that an average harmonic voltage over the bunch train is equal to the required voltage.

Next, we consider that the mth bunch is comprised of a collection of particles. The total rf voltage seen by a particle in the mth bunch is then given by

$$V^{(m)}(\phi) = \mathrm{Re}[\tilde{V}^{(m)}_{c,1} \exp(i\phi) + \tilde{V}^{(m)}_{c,n} \exp(in\phi)]. \tag{20}$$

The longitudinal distribution of particles within the mth bunch is given by [3,11,12]

$$\rho^{(m)}(\phi) = \rho_0 \exp\left(-\frac{1}{\alpha_c^2 \sigma_\varepsilon^2} \Phi^{(m)}(\phi) \right), \tag{21}$$

with

$$\Phi^{(m)}(\phi) = -\frac{\alpha_c}{2\pi h E_0} \int_0^\phi \{e_0 V^{(m)}(\phi') - U_0\} d\phi', \tag{22}$$

where ρ_0 is a normalization constant.

From Eqs. (21) and (22), the shift in the bunch center, $\langle\phi\rangle$, is also derived. This is inconsistent with our initial assumption of equally spaced bunches, which means that our calculation is not self-consistent. In the next subsection, we investigate how this inconsistency affects the calculation results.

D. Comparison with the tracking simulation

First, we applied the semianalytical method to case (iii) in Sec. III B, that is, under the standard fill pattern of the KEK-LS using the TM020-mode third-harmonic cavities. Figure 4 shows the calculated variation in the third-harmonic rf voltage when compared to that from the tracking simulation; in the figure, (a) and (b) indicate

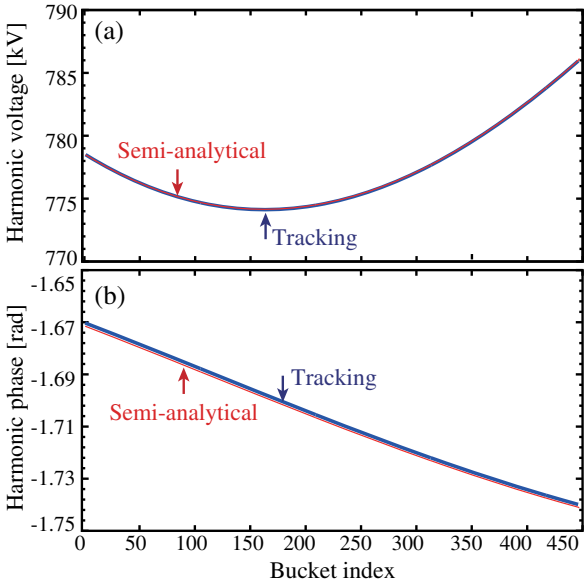

FIG. 4. Variations in the third-harmonic rf voltage due to bunch gaps, which were calculated using the semianalytical method (red) and tracking simulation (blue), respectively. Pictures (a) and (b) show the amplitude and phase, respectively. Abscissa indicates the index of the rf buckets, which ranges over one of the bunch trains. We assumed a beam current of 500 mA with the standard fill pattern of the KEK-LS (two bunch trains, $n_t = 446$, $n_g = 30$).

the amplitude and phase, respectively. Owing to the transient beam loading, both the amplitude and phase changed along the bunch train. As shown in Fig. 4, the semianalytical calculation predicted a very similar harmonic voltage compared to that obtained from the tracking simulation. The relative discrepancy between them was within 0.12%, where the discrepancy was defined by $|\Delta\tilde{V}|/|\tilde{V}|_{\mathrm{av}}$ from the complex voltages, $\Delta\tilde{V}$ and $\tilde{V}$. With a longer bunch-gap of 200 ns, the relative discrepancy was still within 0.14%.

In Fig. 5, we compared the rms bunch lengths that were obtained from the semianalytical calculation and the

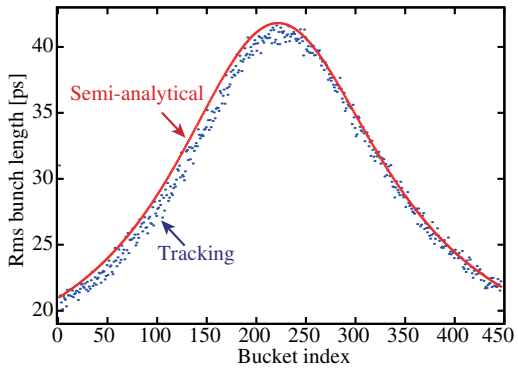

FIG. 5. Comparison of the bunch lengths obtained from the semianalytical calculation (red) and the tracking simulation (blue). Rms bunch lengths along one of the bunch trains are shown. We assumed the same parameters as those in Fig. 4.

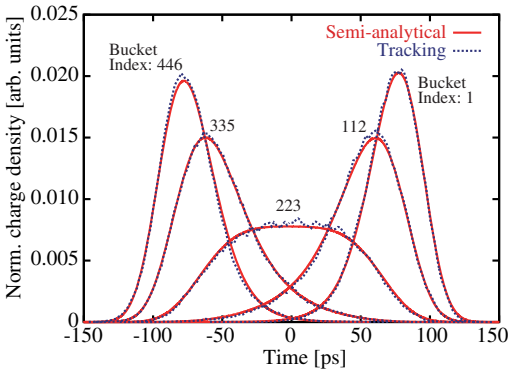

FIG. 6. Typical longitudinal distributions of particles that were predicted by the semianalytical calculation (red) and the tracking simulation (blue). Abscissa indicates the time delay ($= \phi/\omega_{\mathrm{rf}}$). Assumed parameters are the same as in Fig. 5.

tracking simulation, using the same assumptions as those in Fig. 4. Both predictions agreed well within 3%. Figure 6 shows typical longitudinal distributions of particles, which were estimated by the semianalytical method (red) and by the tracking simulation (blue). The distributions in Fig. 6 correspond to the bunch indices of 1, 112, 223, 335, and 446, where indices 1 and 446 correspond to the head and the tail of the bunch train, respectively, while index 223 corresponds to the center of the train where the bunch length was maximum. The particle distributions, which were predicted by the two methods, agreed fairly well.

These examples showed that the semianalytical method can predict the harmonic voltage, bunch length, and longitudinal particle distribution fairly well, at least for the parameters assumed. This suggests that the empty buckets are the primary cause of variations in the main and harmonic rf voltages, while the longitudinal bunch-position shifts affect them only slightly. Then, the bunch lengths will also be evaluated well using a simpler simulation [12] where each bunch is approximated by a point charge. Note that the semianalytical calculations should be verified once again when the bunch gaps are much larger.

E. Estimation of the transient rf voltages

By applying the semianalytical method, we estimated the voltage fluctuations due to bunch gaps in various harmonic cavities. We assumed fill patterns having bunch gaps of 30, 60, and 120 ns, with two bunch trains in the ring. We also assumed the accelerator parameters in Table II with the third-harmonic rf voltage of 777 kV. For the harmonic cavities, we considered the TM020-mode cavity and the other existing 1.5-GHz cavities at the BESSY-II [6], ALS [24], and SLS/ELETTRA [8]. Considering an operating voltage of each cavity given in the references, we chose a reasonable number of cavities, and we assumed the parameters shown in Table IV.

TABLE IV. Parameters of harmonic cavities assumed to estimate the voltage fluctuations.

Cavity	Number	Total R_n/Q (Ω)	Rf voltage per cavity (kV)
TM020-mode	5	386	155
BESSY-II [6]	12	1488	64.8
ALS [24]	7	1126	111
SLS/ELETTRA (SC) [8]	1	176	777

Estimated voltage fluctuations in these cavities are indicated by different symbols in Fig. 7. The voltage fluctuations were defined by $|\Delta\tilde{V}_c|_{max}/|\tilde{V}_c|_{av}$, where $|\Delta\tilde{V}_c|_{max}$ is the maximum deviation of the complex rf voltage and $|\tilde{V}_c|_{av}$ is the average amplitude. Note that this definition includes both amplitude and phase fluctuations. A definition of $|\Delta\tilde{V}_c|_{max}$ is illustrated in Fig. 8.

Let us compare the fluctuations for the typical cavities at a bunch gap of 60 ns. With five TM020-mode cavities, the estimated fluctuation was 7.1% peak-to-peak (p-p). With twelve BESSY-II harmonic cavities, the fluctuation was 35% p-p, which was larger than that of the TM020 cavities by a factor of about 5. With seven ALS harmonic cavities, the fluctuation was 22% p-p. For the SC SLS/ELETTRA cavity, the fluctuation was 3.2% p-p, which was about one half of that of the TM020 cavities.

We also estimated the fluctuations assuming the other parameters of cavities. We assumed three unloaded Q's (Q_0) of 10^4, 4×10^4, and 10^8. For each Q_0, we varied R_n/Q of a single cavity from 20 to 340 Ω in increments of 40 Ω, and we assumed a reasonable number of cavities. Estimated fluctuations for these parameters depended only on the total R_n/Q for a fixed bunch gap, which agreed with a report by Byrd *et al.* [12]. Then, we fitted these fluctuations as a function of R_n/Q, and indicated the fitted curves by dashed lines in Fig. 7. These curves are useful for showing the dependence of the fluctuation on the R_n/Q.

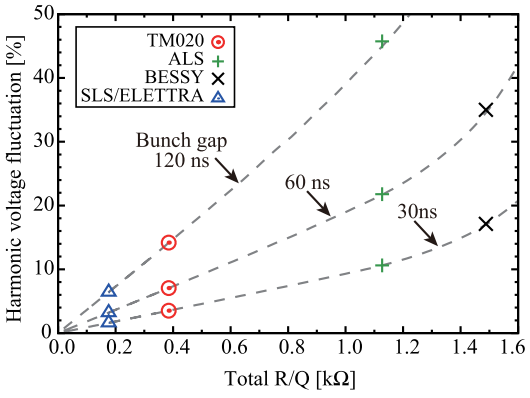

FIG. 7. Estimated fluctuations in the harmonic rf voltage as a function of total R_n/Q. We assumed bunch-gap durations of 30, 60, and 120 ns, and a beam current of 500 mA. The symbols indicate the results for the 1.5-GHz harmonic cavities given in Table IV. Each dashed line represents the curve which fit the results for many sets of parameters with a fixed bunch gap.

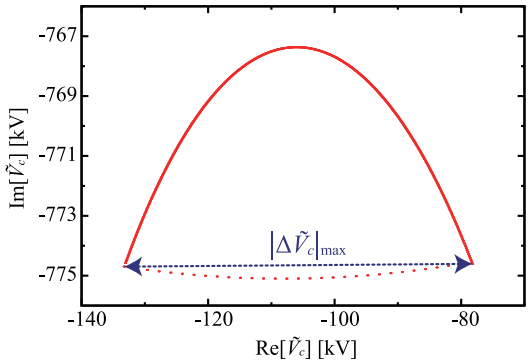

FIG. 8. Definition of the maximum deviation, $|\Delta\tilde{V}_c|_{max}$. Red symbols indicate the harmonic voltages on the complex plane during a period of fill pattern. We assumed a stored current of 500 mA and two 60-ns bunch gaps.

We checked the principal results in Fig. 7 using tracking simulations. With the parameters of ALS cavities and a 120-ns bunch gap, for example, estimated fluctuations were 45.29% (tracking) and 45.21% (semianalytical), respectively, which agreed satisfactorily.

IV. COMPENSATION OF TRANSIENT RF VOLTAGE

The fluctuation in the harmonic voltage can be reduced to typically 7.1% p-p using the TM020-mode cavities. With this small fluctuation, we can further reduce it using an active compensation technique. Here, we present the method involved in this technique, and we investigate its performance, as well as the power and bandwidth needed based on the two measures: (a) compensation on the main and harmonic cavities, and (b) compensation using a separate cavity.

A. Method of compensation

Even when the beam-induced voltage in the harmonic cavities, $\tilde{V}_{b,n}$, fluctuates owing to bunch gaps, we can keep the harmonic voltage constant if we change the generator-induced voltage according to

$$\tilde{V}_{g,n} = (\tilde{V}_{c,n})_{target} - \tilde{V}_{b,n}, \tag{23}$$

where $(\tilde{V}_{c,n})_{target}$ is the target voltage. We consider to conduct this using an active feedforward control. However, owing to the narrow bandwidths of the cavities, this generally requires considerably high peak powers for the generators, which is impractical. Therefore, we need to properly limit the bandwidth of the feedforward control.

Based on the equivalent circuit model [19], the rf voltage in the nth harmonic cavities, $V_{g,n}(t)$, which is induced by

an external generator current of $i_{g,n}(t)$ alone, is given by [25]

$$\frac{d^2V_{g,n}}{dt^2}+\frac{2}{\tau_{f,n}}\frac{dV_{g,n}}{dt}+\omega_{res,n}^2V_{g,n}=2k_n\frac{di_{g,n}}{dt}. \quad (24)$$

We assume the solutions of Eq. (24) in the forms, $V_{g,n}=\tilde{V}_{g,n}(t)e^{in\omega_{rf}t}$ and $i_{g,n}=\tilde{i}_{g,n}(t)e^{in\omega_{rf}t}$, where both $\tilde{V}_{g,n}(t)$ and $\tilde{i}_{g,n}(t)$ are complex functions that vary slowly with time when compared to $e^{in\omega_{rf}t}$. Note that both $\tilde{V}_{g,n}$ and $\tilde{i}_{g,n}$ represent the phasors in a reference frame that is rotating at a frequency $n\omega_{rf}$. Using the assumptions, $(\tau_{f,n})^{-1}\ll n\omega_{rf}$ and $d\tilde{i}_{g,n}/dt\ll n\omega_{rf}\tilde{i}_{g,n}$, we obtain an approximate equation

$$\frac{d\tilde{V}_{g,n}(t)}{dt}+\frac{1}{\tau_{f,n}}(1-i\tan\psi_n)\tilde{V}_{g,n}(t)=k_n\tilde{i}_{g,n}(t). \quad (25)$$

If we specify the required generator voltage $\tilde{V}_{g,n}$, we can deduce the required generator current $\tilde{i}_{g,n}$ using Eq. (25). Conversely, if we specify the generator current $\tilde{i}_{g,n}$, the induced generator voltage is obtained as a solution of Eq. (25) by

$$\tilde{V}_{g,n}(t)=\left[\tilde{V}_{g,n}(-\infty)+k_n\int_{-\infty}^{t}i_{g,n}(t')e^{-\alpha_nt'}dt'\right]\cdot e^{\alpha_nt}, \quad (26)$$

where α_n is given by Eq. (13).

Using the semianalytical method, we can investigate the performance of the band-limited compensation by performing the following steps. (i) From the required generator voltage given by Eq. (23), we deduce the required generator current $\tilde{i}_{g,n}(t)$ using Eq. (25). (ii) We limit the bandwidth of $\tilde{i}_{g,n}(t)$ to a specified value, and obtain $\tilde{i}_{g,n}^{limit}(t)$. (iii) Using Eq. (26), we evaluate a generator-induced voltage $\tilde{V}_{g,n}^{limit}$ that is driven by the band-limited generator current $\tilde{i}_{g,n}^{limit}(t)$. (iv) We obtain an rf voltage under the compensation as $\tilde{V}_{c,n}=\tilde{V}_{g,n}^{limit}+\tilde{V}_{b,n}$. (v) Using the main and harmonic rf voltages obtained, we evaluate the bunch lengths using Eqs. (20)–(22). Note that the rf power required for the generator is given by

$$P_{g,n}(t)=\frac{R_n}{16\beta_n}|\tilde{i}_{g,n}^{limit}(t)|^2. \quad (27)$$

At this moment, we have not determined how to implement the feedforward control to our low-level rf (LLRF) system. A possible solution is reading both fill pattern and beam current in the low-level system, calculating necessary feedforward pattern, and outputting the desired rf signal from the LLRF system.

Using the tracking simulation, we follow the same steps (i)–(iii), and calculate the band-limited generator-voltage $\tilde{V}_{g,n}^{limit}$. Then, we conduct a tracking simulation using that value instead of a constant generator voltage.

The bandwidth of the feedforward control is determined considering the performance of compensation and the peak power required. In the next subsection, we show that with a minimal bandwidth, i.e., the same as a repetition frequency of the bunch trains, we can improve the bunch-lengthening performance.

B. Compensation on the main and harmonic cavities

We investigated the performance of band-limited feedforward compensation with the standard fill pattern of the KEK-LS, that is, two 60-ns bunch gaps at a beam current of 500 mA. The half bandwidth of the compensation was chosen to be 1.1 MHz, which was approximately the same as the repetition frequency of the bunch trains. To limit the bandwidth of $\tilde{i}_{g,n}(t)$, we simply omitted the frequency components outside the bandwidth in its Fourier series. It is worth noting that limiting the bandwidth does not cause any transient behavior because the pattern of $\tilde{i}_{g,n}^{limit}$ is generated in the LLRF system as a feedforward signal. We assumed to compensate both the main and harmonic rf voltages, assuming the parameters in Table III.

Figure 9 shows the results of the semianalytical calculations. The circles in Fig. 9 indicate the rms bunch lengths with the compensation. For reference, those without the compensation are shown by the triangles. Note that the bunch lengths for every five bunches are shown to make the symbols readable. With the compensation, the average bunch length over the bunch trains was improved from 31.1 ps to 34.9 ps. We also confirmed these results by

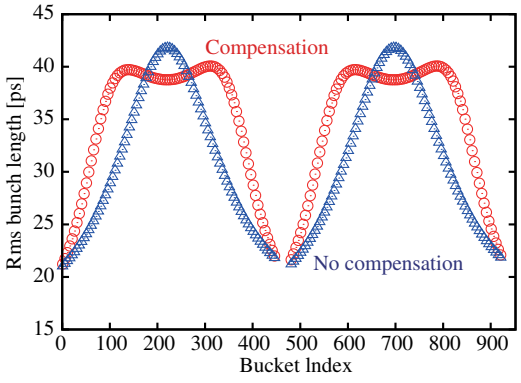

FIG. 9. Rms bunch lengths along the bunch trains with (circles) and without (triangles) the compensation. The bunch lengths are shown at every five buckets. The half bandwidth of the compensation was determined to be 1.1 MHz for both the main and harmonic cavities. We assumed a stored current of 500 mA, two 60-ns bunch gaps, and the parameters of the KEK-LS.

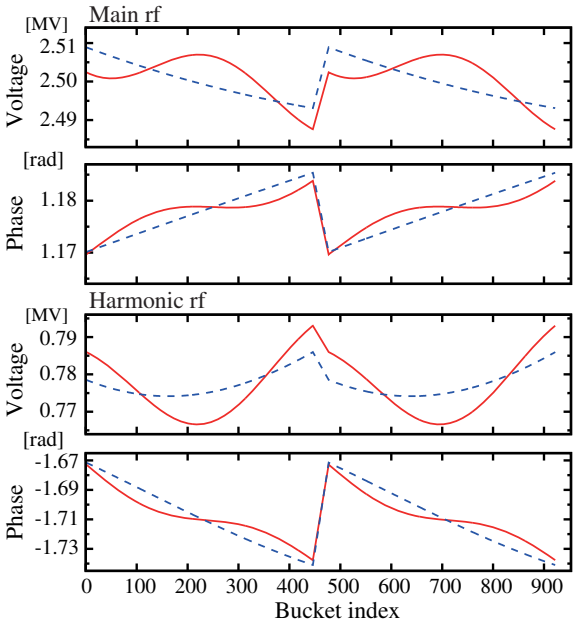

FIG. 10. Rf amplitudes and phases as a function of the bucket index. Solid and dashed lines indicate those with and without the compensation, respectively. The upper two and lower two graphs indicate the main and harmonic rf voltages, respectively.

performing tracking simulations; the average bunch length was 34.2 ps with the compensation.

Figure 10 shows how the amplitude and phase of the rf voltages changed after the compensation (solid lines) when compared to those before compensation (dashed lines). The upper and lower two graphs are for the main and harmonic rf, respectively. Even with the compensation, both the amplitude and phase fluctuated; however, those around the center of each bunch train became closer to the target values given in Table III.

To examine its technical feasibility, we plotted the required power for the generator, as well as the reflected power from the cavity, as a function of time. The solid and dashed lines in Fig. 11 show those with and without the compensation, respectively. The upper two and the lower two graphs represent the main cavity and harmonic cavity, respectively, where the values for a single cavity are indicated. With respect to the main cavity, the peak generator power increased from 131 kW to 149 kW owing to the compensation, while the peak reflected powers were below 11 kW in both cases. For the harmonic cavity, the peak generator power increased from zero to ∼3 kW, while the peak reflected power increased from 4.6 kW to 9.8 kW. All of them are sufficiently feasible.

We also investigated the case where the feedforward half-bandwidth for the main rf was increased to 2.1 MHz. Then, the average rms bunch length was improved to 37.4 ps, while the peak generator power increased to 158 kW per cavity. Therefore, we need to determine the bandwidth considering the required power and the performance.

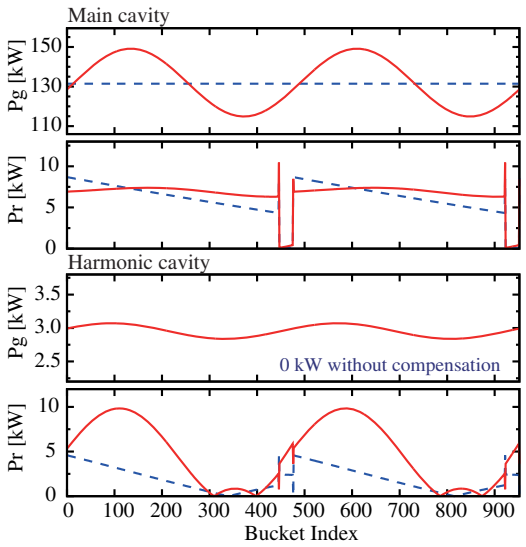

FIG. 11. Required power for the generator (P_g) and reflected power from the cavity (P_r) during a beam revolution period. Both values are for a single cavity. Solid and dashed lines indicate those with and without the compensation, respectively. Upper two graphs are for the main cavity while the lower two are for the harmonic cavity.

C. Compensation using separate rf cavity

If we use a separate cavity to provide the compensation voltage, we can increase the bandwidth of the compensation. A cavity for this purpose should provide an rf voltage that is comparable to the fluctuating rf voltages in the main and harmonic cavities, while keeping its required generator power modest. Considering them, we assumed a 500-MHz cavity having a 3-dB bandwidth of 5 MHz for the compensation cavity. We supposed to use a PF-type cavity, i.e., the same one as the main cavities, while changing its coupling coefficient to 399; the loaded Q was 100 and R/Q was 175 Ω. We also assumed a half bandwidth of 3 MHz for the feedforward compensation. Then, we investigated

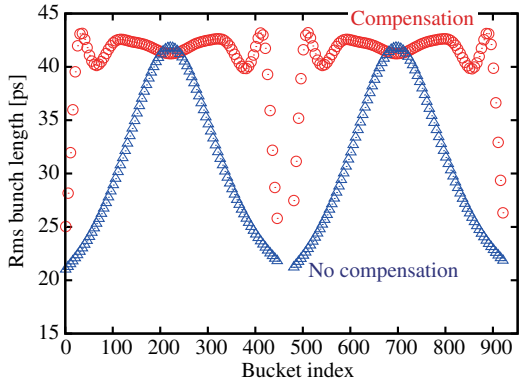

FIG. 12. Rms bunch lengths along the bunch trains with compensation (circles) using a separate cavity when compared to those without compensation (triangles). We assumed a stored current of 500 mA, two 60-ns bunch gaps, and a compensation half-bandwidth of 3 MHz.

its performance assuming the same accelerator parameters as in Sec. IV B.

Figure 12 shows the results of the semianalytical calculations. The circles indicate the rms bunch lengths with the compensation using the separate cavity. As a reference, the triangles indicate those without compensation. The average bunch length over the bunch trains was 40.9 ps, which is close to that (42.5 ps) obtained under ideal conditions without any bunch gaps. The tracking simulation predicted a very similar result; the average bunch length was 40.1 ps with the compensation. The cavity voltage required for this compensation was ∼45 kV, while the peak generator power was ∼50 kW. Both of them are technically feasible.

V. DISCUSSIONS

In the previous sections, we showed that the bunch-lengthening performance can be improved considerably by using the NC TM020-mode harmonic cavities as opposed to conventional NC TM010-mode cavities. In this section, we examine the cases of SC cavities, and then we discuss these performances. We mainly focus on the case of the standard fill pattern (two bunch trains, 60-ns bunch gaps, 500 mA) of the KEK-LS.

When we assumed the SLS/ELETTRA-type [8] SC harmonic cavity, the estimated voltage fluctuation was 3.2% p-p. Combining this cavity with the PF-type main rf cavities, the estimated rms bunch length averaged 35.0 ps.

We further considered to use the SC cavities for the main rf system. We assumed to use two KEKB-type SC cavities [26], each having an unloaded Q of 2×10^8 and an R/Q of 93 Ω. With these cavities, the voltage fluctuation was estimated to be 0.4% p-p. Assuming these SC main cavities and the SLS/ELETTRA-type SC harmonic cavity, the estimated average bunch length was 39.7 ps.

Table V shows a summary of the estimated bunch lengths based on the semianalytical calculations. We expect the average bunch length of 40.9 ps using the TM020-mode harmonic cavities and the PF-type main cavities, along with an active compensation using a separate cavity. This bunch length is 96% of that obtained under ideal conditions without any bunch gaps. It is also comparable to the bunch length of 39.7 ps that is expected with a full SC double-rf system. Therefore, if the active compensation is applied, the NC double-rf system can provide a bunch-lengthening performance that is comparable to that obtained with the SC double-rf system, at least, with an assumed bunch gap of 60 ns.

A liquid-Helium refrigerator system, which is needed for the SC cavities, requires considerable construction and operation costs, as well as substantial effort to observe the high-pressure regulations. The SC cavities are also very sensitive to any contamination of microparticles and to the condensation of residual gas on their surface; this therefore requires significant work to operate them. On the other hand, the NC cavities are less expensive, robust against contaminations, and convenient. Considering these issues and the performances, the NC double-rf system based on the TM020-mode cavities is considered a very attractive solution for lengthening the bunches in next-generation light sources. However, for some specific fill patterns, such as a hybrid fill pattern comprised of an isolated bunch and a train of multi-bunches, the SC system may be advantageous.

TABLE V. Summary of the average rms bunch lengths that were estimated with semianalytical calculations. We assumed a beam current of 500 mA, two bunch trains, 60-ns bunch gaps, and the KEK-LS parameters.

Main cavity (500 MHz)	Harmonic cavity (1.5 GHz)	Average bunch length (ps)
NC	-	9.5[a]
NC	NC TM010	17.1
NC	NC TM020	31.1
NC	NC TM020 with Comp.[b]	34.9
NC	SC TM010	35.0
NC	NC TM020 with Comp.[c]	37.4
SC	SC TM010	39.7
NC	NC TM020 with Comp.[d]	40.9
NC	NC TM020 without bunch gaps	42.5

[a]Natural bunch length.
[b]Compensation on the main and harmonic cavities with 1.1-MHz bandwidth.
[c]Compensation on the main and harmonic cavities with 2.1-MHz and 1.1-MHz bandwidths, respectively.
[d]Compensation using a separate rf cavity with 3-MHz bandwidth.

In Secs. II B and III C, we simplified our expressions by setting the bunch form factor F to be 1. This was justified by the good agreements between the semianalytical and tracking simulations for the examined cases. However, if the bunches are much longer, we should modify some of the expressions to include the form factor. A detailed discussion related to the form factor was presented in [11].

In this study, we ignored the effects of the coupling impedance of vacuum components. In particular, an inductive wakefield can produce a slope in the rf voltage, and this can affect the bunch lengthening. We believe that with an active double-rf system, we can cancel such a slope by modifying our operating conditions. However, this issue should be investigated in the future. The microwave instability due to the longitudinal impedance is another important issue to be investigated. We also need to examine the effect of amplitude and phase errors of rf voltages on the bunch-lengthening performance.

To compensate the transient voltages, the bandwidths of rf generators should be sufficiently wider than the assumed half-bandwidths, 1–3 MHz, of the feedforward compensation. It is somewhat difficult to achieve these bandwidths using klystrons, but it is feasible with high-power solid-state amplifiers. For example, we obtained a 1-dB bandwidth of about 10 MHz with our prototype 1-kW, 500-MHz solid-state amplifier.

As was noted in Sec. IV A, we have not performed a concrete design of low-level rf system. The LLRF system should provide an rf signal including a fast feedforward pattern to compensate the transients while stabilizing both amplitude and phase of rf voltage on average using some feedback loops. We believe that both the feedforward and the feedback will be realized compatibly if they have much different response times, however, an implementation of such functions in the LLRF system should be investigated hereafter.

Finally, we discuss some operational aspects of a proposed double rf system. As shown in Fig. 9, the bunches are less lengthened, and thus have short Touschek lifetimes, in both head and tail of a bunch train. In order to keep the fill pattern still, we need to replenish these bunches with the top-up injection. We should also note that the harmonic rf produces a large synchrotron-tune spread. In addition, when the bunch gaps exist, the synchrotron tune can depend on the index of bunches. These issues might impose challenges in designing a longitudinal bunch-by-bunch feedback system, and should be investigated in the future.

VI. CONCLUSIONS

To lengthen the beam bunches in the next-generation light sources, we proposed an NC double-rf system that is based on 1.5-GHz TM020-mode harmonic cavities. Owing to their low R/Q and high unloaded Q, the TM020-mode cavities are very effective in reducing the transient variations in the harmonic rf voltages, which are induced by bunch gaps. Assuming a typical bunch-gap duration of 60 ns, together with the parameters of the proposed KEK-LS, the fluctuation in the harmonic rf voltage is estimated to be 7.1% p-p, which is considerably smaller than that estimated for conventional TM010-mode harmonic cavities, i.e., 22–35% p-p. Using the TM020-mode harmonic cavities, we expect an average rms bunch length of 31 ps, which is longer than the natural one by a factor of 3.3.

Once the voltage fluctuation is reduced, we can further improve the bunch lengthening using active compensation techniques within technical feasibility. If we use a separate rf cavity for the compensation, we expect an average bunch length of 40.9 ps, which is comparable to what is expected with a full SC double-rf system. Then, the NC double-rf system, based on the TM020-mode cavities, is a very attractive solution for light sources, at least for a modest bunch-gap duration of ~60 ns.

To perform this study, we developed a macroparticle tracking code that can incorporate the effect of the active compensation technique. We also developed a semianalytical method to calculate the bunch lengths and transient rf voltages. We showed that these semianalytical calculations predict very similar results to those from tracking simulations within the range of parameters that we examined. The semianalytical method helps us understand the simulation results, and it is useful for performing a quick survey of multiple cases.

ACKNOWLEDGMENTS

This work was supported by Japan Society for the Promotion of Science (JSPS) KAKENHI Grant No. JP17K05131.

[1] L. Liu and H. Westfahl, Jr., Towards diffraction limited storage ring based light sources, in *Proceedings of the 8th International Particle Accelerator Conference, IPAC'17, Copenhagen, Denmark, 2017* (JACoW, Geneva, 2017), p. 1203.

[2] S. C. Leemann, Interplay of Touschek scattering, intrabeam scattering, and rf cavities in ultralow-emittance storage rings, Phys. Rev. Accel. Beams **17**, 050705 (2014).

[3] A. Hofmann and S. Myers, CERN, Technical Report No. CERN-ISR-TH-RF/80-26, 1980.

[4] J. M. Byrd, S. De Santis, M. Georgsson, G. Stover, J. D. Fox, and D. Teytelman, Commissioning of a higher harmonic RF system for the Advanced Light Source, Nucl. Instrum. Methods Phys. Res., Sect. A **455**, 271 (2000).

[5] M. Georgsson, W. Anders, D. Krämer, and J. M. Byrd, Design and commissioning of third harmonic cavities at BESSY II, Nucl. Instrum. Methods Phys. Res., Sect. A **469**, 373 (2001).

[6] W. Anders and P. Kuske, HOM damped NC passive harmonic cavities at BESSY, in *Proceedings of the 2003 Particle Accelerator Conference, PAC 2003, Portland, U.S.A., 2003* (IEEE, New York, 2003), p. 1186.

[7] M. Pedrozzi, J. Raguin, W. Gloor, A. Anghel, M. Svandrlik, G. Penco, P. Craievich, A. Fabris, C. Pasotti, E. Chiaveri, R. Losito *et al.*, SLS operational performance with third harmonic superconducting system, in *Proceedings of the 11th Workshop on RF Superconductivity, Lübeck/Travemünde, Germany* (2003), p. 91, http://accelconf.web.cern.ch/Accelconf/SRF2003/papers/mop25.pdf.

[8] P. Bosland, P. Brédy, S. Chel, G. Devanz, M. Luong, P. Craievich, G. Penco, M. Svandrlick, M. Pedrozzi, W. Gloor *et al.*, Third harmonic superconducting passive cavities in ELETTRA and SLS, in *Proceedings of the 11th Workshop on RF Superconductivity, Lübeck/Travemünde, Germany* (2003), p. 239, http://accelconf.web.cern.ch/Accelconf/SRF2003/papers/tuo06.pdf.

[9] G. Penco and M. Svandrlik, Experimental studies on transient beam loading effects in the presence of a superconducting third harmonic cavity, Phys. Rev. Accel. Beams **9**, 044401 (2006).

[10] N. Milas and L. Stingelin, Impact of filling patterns on bunch length and lifetime at the SLS, in *Proceedings of the first International Particle Accelerator Conference, IPAC'10, Kyoto, Japan* (IPAC'10/ACFA, Kyoto, 2010), p. 4719.

[11] P. F. Tavares, Å. Andersson, A. Hansson, and J. Breunlin, Equilibrium bunch density distribution with passive harmonic cavities in a storage ring, Phys. Rev. Accel. Beams **17**, 064401 (2014).

[12] J. M. Byrd, S. De Santis, J. Jacob, and V. Serriere, Transient beam loading effects in harmonic rf systems

for light sources, Phys. Rev. Accel. Beams **5**, 092001 (2002).

[13] H. Ego, J. Watanabe, S. Kimura, and K. Sato, Design of a HOM-damped rf cavity for the SPring-8-II storage ring, in *Proceedings of the 11th Annual Meeting of Particle Accelerator Society of Japan, Aomori, Japan* (PASJ, Tokyo, 2014), p. 237 [http://www.pasj.jp/web_publish/pasj2014/proceedings/PDF/MOOL/MOOL14.pdf].

[14] Y. Asano *et al.*, SPring-8-II Conceptual Design Report (RIKEN SPring-8 Center, 2014), p. 56 [http://rsc.riken.jp/pdf/SPring-8-II.pdf].

[15] K. Harada, T. Honda, Y. Kobayashi, N. Nakamura, K. Oide, H. R. Sakai, S. Sakanaka, M. Adachi, K. Tsuchiya, and N. Funamori, The HMBA lattice optimization for the new 3 GeV light source, in *Proceedings of the 7th International Particle Accelerator Conference, IPAC'16, Busan, Korea, 2016* (JACoW, Geneva, 2016), p. 3251.

[16] T. Honda, Concept of a new generation synchrotron radiation facility KEK light source, in *Proceedings of the 8th International Particle Accelerator Conference, IPAC'17, Copenhagen, Denmark, 2017* (JACoW, Geneva, 2017), p. 2687.

[17] T. Takahashi, S. Sakanaka, and N. Yamamoto, Design study of damped accelerating cavity based on the TM020-mode and HOM couplers for the KEK light source project, in *Proceedings of the 8th International Particle Accelerator Conference, IPAC'17, Copenhagen, Denmark, 2017* (JACoW, Geneva, 2017), p. 4172.

[18] K. Halbach and R. F. Holsinger, SUPERFISH-a computer program for evaluation of RF cavities with cylindrical symmetry, Part. Accel. **7**, 213 (1976).

[19] P. B. Wilson and J. E. Griffin, High energy electron linacs; application to storage ring RF systems and linear colliders, in *AIP Conference Proceedings*, Vol. 87, edited by R. A. Carrigan, F. R. Huson, and M. Month (AIP, 1982), p. 450.

[20] M. Izawa, T. Koseki, S. Sakanaka, T. Takahashi, K. Hass, S. Tokumoto, and Y. Kamiya, Installation of new damped cavities at the Photon Factory storage ring, J. Synchrotron Radiat. **5**, 369 (1998).

[21] V. Serrière and J. Jacob, Expected lifetime improvement with a superconducting harmonic RF system at the ESRF, in *Proceedings of the 8th European Particle Accelerator Conference, Paris, 2002* (EPS-IGA and CERN, Geneva, 2002), p. 748.

[22] G. Skripka, R. Nagaoka, M. Klein, F. Cullinan, and P. F. Tavares, Simultaneous computation of intrabunch and interbunch collective beam motions in storage rings, Nucl. Instrum. Methods Phys. Res., Sect. A **806**, 221 (2016).

[23] M. Pedrozzi, W. Gloor, A. Anghel, M. Svandrlik, G. Penco, P. Craievich, A. Fabris, C. Pasotti, E. Chiaveri, R. Losito, S. Marque, O. Aberle, P. Marchand, P. Bosland, S. Chel, P. Brédy, and G. Devanz, First operational results of the 3rd harmonic super conducting cavities in SLS and ELETTRA, in *Proceedings of the 2003 Particle Accelerator Conference, PAC 2003, Portland, U.S.A., 2003* (IEEE, New York, 2003), p. 878.

[24] J. Byrd, K. Baptiste, S. De Santis, S. Kosta, C. C. Lo, D. Plate, R. A. Rimmer, and M. Franks, Design of a higher harmonic RF system for the Advanced Light Source, Nucl. Instrum. Methods Phys. Res., Sect. A **439**, 15 (2000).

[25] S. Sakanaka, Investigation of bunch-gap effects for curing ion trapping in energy recovery linacs, in *Proceedings of 41st Advanced ICFA Beam Dynamics Workshop on Energy Recovery Linacs, ERL07, Daresbury, UK, 2007*, p. 41, http://accelconf.web.cern.ch/AccelConf/erl07/papers/15.pdf.

[26] T. Furuya, K. Akai, K. Hara, K. Hosoyama, A. Kabe, Y. Kojima, S. Mitsunobu, Y. Morita, H. Nakai, and T. Tajima, Recent status of the superconducting cavities for KEKB, in *Proceedings of the 9th Workshop on RF Superconductivity, Santa Fe, U.S.A., 1999*, p. 31, https://accelconf.web.cern.ch/accelconf/SRF99/papers/mop001.pdf.